Electronic Supplementary Information for

Two-color Sum Frequency Generation Study of poly(9,9-dioctylfluorene)/Electrode Interfaces

Takayuki Miyamae,* Kiyomi Tsukagoshi and Wataru Mizutani

1. Experimental Section

1.1 Sample preparation

The samples of the PFO endcapped with dimethylphenyl (MW=48.8K) were obtained from American Dye Source and used as received. At first, thin film of the filtered PEDOT:PSS solution (CREVIOS Al4083) was spin-coated at 3000 rpm on the top of the fused quartz or 2 mm thick CaF_2 (Pier Optics Co.) substrates and then baked at 150 °C for 60 min in an oven with N_2 flow. PFO layer was then spin-coated at 3000 rpm from 1% w/v toluene solution through a 0.4μm filter on top of the PEDOT:PSS layer. Then the films were evacuated to eliminate residual solvent.

For the measurements of the buried electrode/PFO interface, the LiF and the Al were directly deposited on the spin-coated PFO/PEDOT:PSS onto 2 mm thick CaF_2 substrates in a vacuum chamber with base pressure of 1×10^{-7} Pa. A pumping system was composed of a 2000 l/s turbomolecular pump and a 500 l/min rotary pump for a vacuum deposition chamber and a 50 l/s turbomolecular pump and a 90 l/min rotary pump for a load-lock chamber. The thicknesses of the LiF and Al are about 1 and 40 nm, respectively. The thicknesses of Al and LiF films were monitored using a quartz microbalance. The deposition rate of the sample materials, were about 0.5-1.5 nm/s for Al and 0.01nm/s for LiF, respectively.

1.2 Two-color SFG measurements

The basic SFG system employed in this experiment has been described in detail in the previous publication,[1.] and we modified this system for the two-color experiment.[2.] In brief, a mode-locked Nd:YAG laser (Ekspla, PL-2143D, 25ps pulsewidth, 10Hz) with two optical parametric systems (Ekspla, DFG401) was used to generate a tunable visible beam from 420 to 640 nm and a tunable IR beam from 2.5 to 10 μm. The visible and IR beams were overlapped at sample surface with the incidence angles of 70° and 50°, respectively. The spectral resolution of the IR beam was 6 cm^{-1}, and the IR frequency was calibrated with the absorption lines of polystyrene standard. In order to minimize the irradiation damage, both IR and visible beams were defocused. The focus size of the IR and visible beams were >1 mm and >3 mm, respectively. Further, in order to avoid

photo-irradiated damage, the fluence of the visible beam was kept below 50 μJ and 10 μJ per pulse for the PFO surface and the electrode/PFO interface, respectively. The sum-frequency output signal was filtered with short-wave-pass filters, monochromator (Oriel MS257), and then detected by a photomultiplier tube. The signal was then averaged over 300 pulses by a gated integrator for every data point taken at a 5 cm^{-1} interval and was stored in a personal computer. All SFG intensities were normalized using a z-cut quartz crystal. In the frequency region between 2000 and 1300 cm^{-1}, significant portion of the infrared beam is absorbed by water vapour in the optical path. The effect was minimized by purging the optical path of the IR beam and the sample stage by dry nitrogen gas.

2. Theory of the doubly-resonant SFG

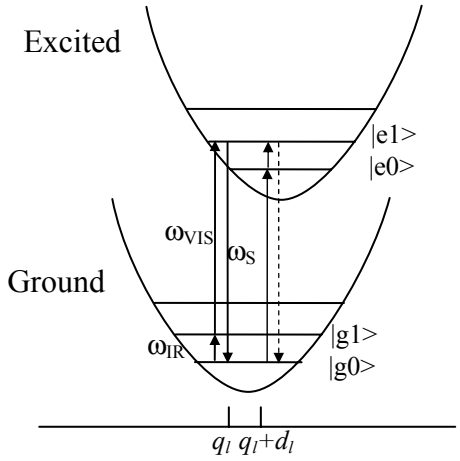

Fig. S1. Energy diagram for doubly-resonant SFG. The vibration harmonic potentials are shifted between the ground and excited states. The resonant transitions involved in the doubly resonant IR–visible (and visible–IR) sum-frequency generation processes are shown schematically.

In the infrared–visible (and visible–infrared) doubly–resonant (DR) SFG process shown schematically in Fig. S1, the microscopic expression for $\chi^{(2)}$ is dominated by doubly resonant terms. In the dipolar electric approximation, SFG is forbidden in centrosymmetric materials, but not at their interfaces, where the inversion symmetry of the bulk is broken. For such an air–metal interface, the SFG intensity reflected from the surface is given by

$$I(\omega_{SF}) \propto \left| \chi^{(2)}_{eff} : E(\omega_{IR}) E(\omega_{VIS}) \right|^2 \qquad \text{(S1)}$$

$\chi^{(2)}_{eff}$ is the effective second-order nonlinear susceptibility tensor and $E(\omega_{IR})$ and $E(\omega_{VIS})$ are the input fields.

The adsorbate nonlinear susceptibility contains nonresonant, singly resonant, and doubly resonant contributions. The latter dominates strongly if the vibrations (ω_l) and electronic transitions

(ω_{eg}) probed by ω_{IR} and ω_{SFG} are coupled. Both IR–visible and visible–IR processes contribute to doubly–resonant SFG. However, the IR–visible sequence is expected to dominate, as a result of the quicker relaxation of the electronic excitation compared to the vibrational one. Assuming harmonic potential surfaces for the electronic states and the Born–Oppenheimer and Condon approximations, the IR–visible doubly–resonant $\chi^{(2)}_{eff}$ can be described as[3.,4.]

$$\chi^{(2)}_{ijk} = -\frac{N}{\hbar^2}\left\langle \mu^i_{eg}\mu^j_{eg}\frac{\partial \mu^k_{gg}}{\partial q_l}\frac{\sqrt{S_l}e^{-S_l}}{\omega_{\mathrm{IR}}-\omega_l+i\Gamma_l} \times\sum_{n=0}^{\infty}\frac{S_l^n}{n!}\left\{\frac{1}{\omega_s-n\omega_l-\omega_{eg}+i\Gamma_{en,g0}}-\frac{1}{\omega_s-(n+1)\omega_l-\omega_{eg}+i\Gamma_{en+1,g0}}\right\}\right\rangle+\chi^{(2)}_{NR,ijk} \qquad \text{(S2)}$$

where N is the surface molecular density, $\mu_{eg}{}^{i}$ represents the i component of electronic transition moment, q_l is the normal coordinate, S_l is a dimensionless coupling constant known as the Huang-Rhys factor, n labels the vibrational state, g and e label the ground and excited electronic states, respectively, ω_{SFG} is the SFG frequency, ω_l and ω_{eg} are the resonant vibrational and electronic frequencies, respectively, Γ_l and $\Gamma_{en,g0}$ are the damping constants, the angular brackets indicate an average over molecular orientations, and $\chi^{(2)}_{NR,ijk}$ describes the non-resonant contributions. S_l is related to the shift d_l of the harmonic potential of the vibration in the excited electronic level by

$$S_l = \frac{1}{2\hbar}\omega_l d_l^2 . \qquad \text{(S3)}$$

As shown in Fig. S1, DR-SFG occurs thus for $\omega_{IR} = \omega_l$ and for several visible frequencies, when, ω_{SFG} matches an allowed vibronic transition to the excited electronic level. The intensity of each vibronic resonance depends on the Frank-Condon overlap integrals of the vibrational levels involved in the transition. Since the initial and final vibrational states, respectively of the visible and SFG transitions, always differ (see Fig. S1), the vibration and the electronic transition must therefore be coupled ($d_l \neq 0$) to have a non-zero transition probability for the global DR-SFG process. Thus the DR-SFG spectrum allows for the determination of the coupling strength and characteristics.

Equation S2 includes all the vibronic transitions series. However, in general, the VIS-IR SFG is much weaker and not detected because of the very fast relaxation of the electronic excitation. Actually, the dephasing times of vibronic transitions are in the femtosecond region for PFO.[5.] Therefore, by assuming $\Gamma_{en,g0} >> \Gamma_{e0,g0}$, the nonzero vibronic transitions can be neglected.

It is worth pointing out that a significantly larger $\Gamma_{en,g0}$ also suppresses the aforementioned VIS-IR SFG, which starts with an electronic transition followed by a vibrational transition.

To analyze the spectra, we note that with the visible input frequency ω_{vis} fixed, Eq. (S3) can be approximated by the form

$$\chi^{(2)}_{ijk} \propto \sum_l \frac{A_l}{\omega_{\mathrm{IR}}-\omega_l+i\Gamma_l}+\chi^{(2)}_{NR}e^{i\xi}, \qquad \text{(S4)}$$

with A_l describing the electronic resonance. We use Eq. S4 to fit all the measured spectra with ω_l, Γ_l, A_l,ξ , and $\chi^{(2)}_{NR}$ as adjustable parameters.

3. Fitting Summary

TABLE S1: Fitting Parameters of the SSP SFG Data from Figure 1.[a]

Visible (nm)	$\chi_{NR,ijk}$	ξ	A_l	error bar
420	0.301	107	8.92	1.338
425	0.360	102	9.11	1.367
435	0.688	105	10.86	1.629
440	0.474	101	10.19	1.529
450	0.498	99	8.02	1.203
470	0.248	92	6.02	0.903
490	0.122	81	4.05	0.608
500	0.197	72	2.74	0.411
510	0.160	60	2.62	0.393
520	0.142	62	1.88	0.282
532	0.111	66	1.59	0.239
550	0.180	66	0.78	0.117
570	0.128	56	0.53	0.080

[a] Peak position ω_l and the width Γ_l are fixed with 1610 cm^{-1} and 8 cm^{-1}, respectively.

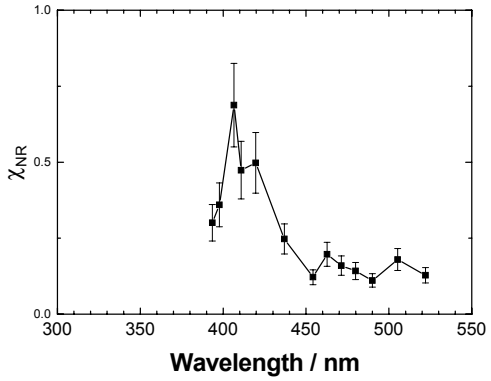

Figure S2 The changes in the χ_{NR} deduced from the fitting of the two-color SFG spectra in Fig. 1.

TABLE S2: Fitting Parameters of the SSP SFG Data from Figure 2.[b]

Visible (nm)	$\chi_{NR,ijk}$	ξ	A_l	error bar
420	0.466	10	1.90	0.38
435	0.664	13	3.40	0.67
440	0.560	16	4.06	0.83
450	0.624	15	4.60	0.67
470	0.490	16	2.95	0.65
490	0.273	10	1.91	0.38
510	0.207	5	0.80	0.11
532	0.126	-5	1.05	0.15

[b] Peak position ω_l and the width Γ_l are fixed with 1610 cm^{-1} and 8 cm^{-1}, respectively.

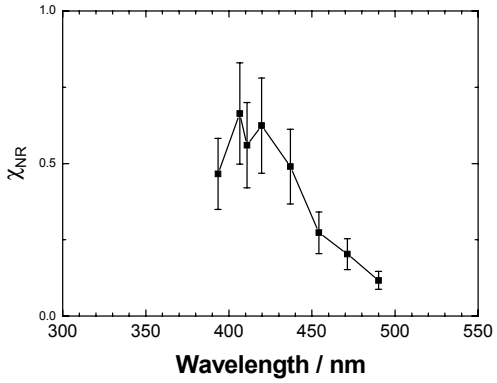

Figure S3 The changes in the χ_{NR} deduced from the fitting of the two-color SFG spectra in Fig. 2.

References

1. T. Miyamae, K. Tsukagoshi, O. Matsuoka, S. Yamamoto, and H. Nozoye, *Langmuir,* 2001, **17**, 8125.
2. T. Miyamae, Y. Miyata, and H. Kataura, *J. Phys. Chem. C*, 2009, **113**, 15314.
3. M. B. Raschke, M. Hayashi, S. H. Lin, and Y. R. Shen, *Chem. Phys. Lett.*, 2002, **359**, 367.
4. M. Hayashi, S. H. Lin, M. B. Raschke, and Y. R. Shen, *J. Phys. Chem*. A 2002**, 106**, 2271
5. T. Virgili, D. G. Lidzey, D. D. C. Bradley, G. Cerullo, S. Stagira, and S. De Silvestri, *Appl. Phys. Lett.*, 1999, **74**, 2767.